iScience

Article

Decoding unchanged transcriptome of Alzheimer's disease reveals an NCAM1 mRNA switch as a potential biomarker

Graphical abstract

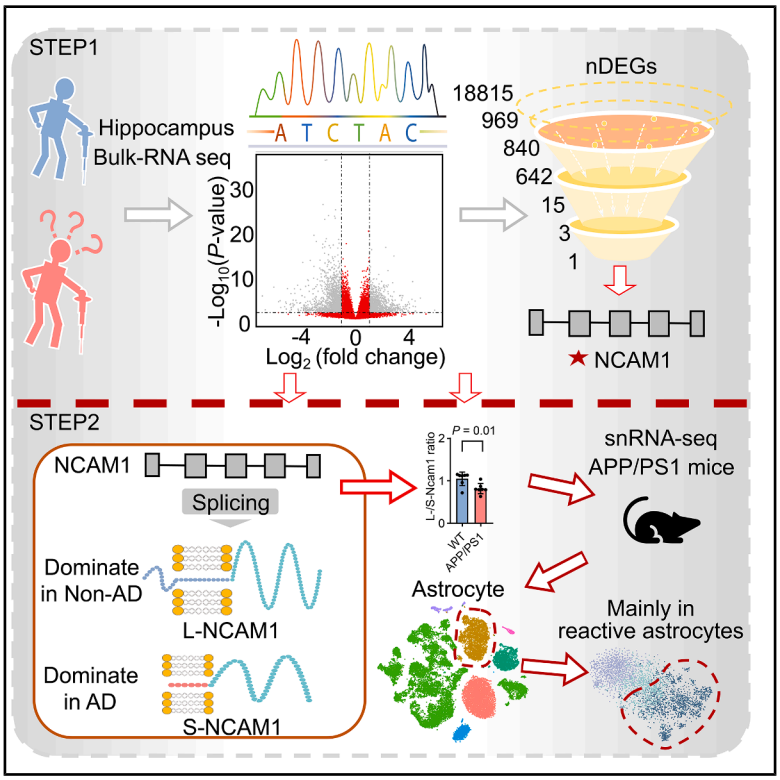

Highlights

- Hippocampal transcriptome analysis identified 15 candidate AD biomarkers
- NCAM1 was identified as a key candidate and validated in APP/PS1 mice
- snRNA-seq showed NCAM1 isoform switching mainly in activated astrocytes

Authors

Haotian Li, Sai Liu, Daoxin Miao, ..., Zheying Zhu, Xinuo Li, Qiulun Lu

Correspondence

guangjiwang@hotmail.com (G.W.), zheying.zhu@nottingham.ac.uk (Z.Z.), xinuo.li@cpu.edu.cn (X.L.), qiulunlu@cpu.edu.cn (Q.L.)

In brief

Health sciences; Neuroscience; Molecular neuroscience; Clinical neuroscience; Cellular neuroscience

Li et al., 2026, iScience *29*, 115456
April 17, 2026 © 2026 The Author(s). Published by Elsevier Inc.
https://doi.org/10.1016/j.isci.2026.115456

CellPress

iScience

CellPress
OPEN ACCESS

Article

Decoding unchanged transcriptome of Alzheimer's disease reveals an NCAM1 mRNA switch as a potential biomarker

Haotian Li,[1,3] Sai Liu,[1,3] Daoxin Miao,[1] Long Chen,[1] Yuan Sun,[1] Guangji Wang,[1,*] Zheying Zhu,[2,*] Xinuo Li,[1,*] and Qiulun Lu[1,4,*]

[1]State Key Laboratory of Natural Medicines, China Pharmaceutical University, Nanjing 211198, China
[2]School of Pharmacy, The University of Nottingham, NG72RD Nottingham, UK
[3]Senior author
[4]Lead contact
*Correspondence: guangjiwang@hotmail.com (G.W.), zheying.zhu@nottingham.ac.uk (Z.Z.), xinuo.li@cpu.edu.cn (X.L.), qiulunlu@cpu.edu.cn (Q.L.)
https://doi.org/10.1016/j.isci.2026.115456

SUMMARY

Alzheimer's disease (AD), a neurodegenerative disease primarily affecting older adults, is characterized by changes in memory, behavior, and language. Although gene expression varies during AD progression, the molecular mechanisms underlying this variation remain unclear. RNA sequencing indicates that most genes exhibit minimal gene-level differential expression in AD but may relate to neuronal function. Our comprehensive analysis revealed that neural cell adhesion molecule 1 (NCAM1) underwent alternative splicing (AS) in AD. Notably, an isoform switch occurred from the long isoform (L-NCAM1), typical under normal conditions, to the short isoform (S-NCAM1) in AD. S-NCAM1 lacked the intracellular domain in L-NCAM1. Additionally, the S-NCAM1-to-L-NCAM1 ratio increased in the hippocampus of amyloid precursor protein (*APP*)/PS1 mice compared to wild-type mice. Single-nucleus sequencing determined that this change in NCAM1 isoforms occurred predominantly within reactive astrocytes. Hence, AS may play a key role in AD development, while the L-NCAM1-to-S-NCAM1 ratio could serve as a biomarker.

INTRODUCTION

Population aging has resulted in a heightened prevalence of neurodegenerative diseases, many of which manifest clinically as dementia. Alzheimer's disease (AD) is the leading cause of dementia, responsible for approximately 60–80% of cases globally.[1–3] AD is a progressive neurodegenerative disorder characterized by damaged brain cells, which leads to cognitive decline, memory impairment, and deficits in language abilities.[4] Pathologically, AD is characterized by the extracellular accumulation of β-amyloid (Aβ) and the formation of intracellular neurofibrillary tangles (NFTs) composed of hyperphosphorylated tau. These biomarkers are commonly observed in individuals experiencing memory deficits and progressive cognitive deterioration.[2,4,5]

During AD progression, alterations in gene expression profiles lead to changes in enzyme activity that correlate with disease severity.[6,7] Notably, the aberrant expression of genes, such as amyloid precursor protein (*APP*), presenilin 1 (*PSEN1*), and presenilin 2 (*PSEN2*), contributes to increased Aβ production and aggregation.[8,9] While significant advancements have been achieved in elucidating the molecular pathogenesis of AD, its complete etiology and mechanisms of progression remain incompletely understood.

Recent research has highlighted that post-transcriptional modifications (PTMs) are linked to disease states.[10] While translation levels are maintained, post-translational modification—a classical type of PTM—plays a key role in regulating protein function. Additionally, two main regulatory mechanisms at the transcriptional level, mRNA splicing and mRNA modulation, also impact which proteins are ultimately produced by altering translation products and thus protein activity. As genes are transcribed into precursor messenger RNA (pre-mRNA), mature mRNA is produced after intron splicing, enabling translation into specific proteins.[11]

Throughout mRNA maturation, certain exons can be selectively included or excluded via alternative splicing (AS), a critical process that allows a single gene to generate multiple protein isoforms with distinct properties.[12–14]

Substantial evidence indicates that AS plays a critical role in AD pathology, while previous studies have largely focused on splicing events in selected candidate genes.[15] For instance, tau is a well-established pathological hallmark of AD encoded by the microtubule-associated protein tau (*MAPT*) gene; disruptions to *MAPT* splicing can alter tau isoform abundance, closely associated with tau pathology accumulation in AD.[16] Additionally, Lambert et al. demonstrated that bridging integrator 1 (BIN1) isoform 1 (*BIN1* iso1) contributes to early endosome size dysregulation,

This is an open access article under the CC BY-NC-ND license (http://creativecommons.org/licenses/by-nc-nd/4.0/).

an early pathophysiological feature of AD.[17] More comprehensive analyses have also revealed widespread dysregulation of mRNA splicing in AD, leading to the identification of several AD-associated genes and emphasizing the value of global transcriptome splicing analyses.[15] Notably, although *MAPT* and *BIN1* are among the most extensively researched AD-related genes, neither has exhibited significant overall expression changes—defined as an absolute log2 fold change greater than 1 and a *p*-value below 0.05—in multiple bulk RNA-seq datasets from human brain tissue.[18,19] This highlights the need to explore AS events and pathology-associated isoforms in genes that show no significant changes in total expression in transcriptomic analyses.

Accordingly, in the current study, we analyzed alterations in AS profiles under AD conditions by examining human brain tissues and identifying cell-type-specific AS events that occur during AD progression. This strategy enabled the elucidation of regulatory mechanisms underlying AS in genes with stable expression levels, thereby supporting the identification of biomarkers relevant to AD therapy.

RESULTS

Gene-level non-differentially expressed genes (nDEGs) are associated with AD

This study examined the biological functions of genes without differential expression in AD. To this end, we analyzed a bulk RNA-seq dataset (GSE173955) from the hippocampi of 8 individuals diagnosed with AD and 10 non-AD controls.[20] Both groups comprised individuals aged 65 years or older with comparable male-to-female ratios (Figures 1A and 1B). Upon alignment to the human genome, we identified 21,506 genes; among these, 1,243 were significantly downregulated and 1,448 were upregulated in the AD group. Thus, DEGs constituted only 12.5% of all genes, leaving 18,815 gene-level non-differentially expressed genes (nDEGs) (Figure 1C and Table S1), based on an absolute log2 fold change over 1 and a *p*-value below 0.05.

The potential involvement of the predominant nDEGs in AD pathogenesis was investigated using Proteomaps functional enrichment analysis, which identified subsets of nDEGs associated with neurodegenerative diseases (Figure 1D). Further Gene Ontology (GO)-based enrichment analyses of nDEGs and DEGs (Figure 1E) highlighted several pathways relevant to neuronal function, including the regulation of transport, dendrite development, neuronal apoptosis, and neuronal projection—all critical for neural integrity and injury responses.

Notably, DEGs comprised a small fraction of these pathways, whereas most genes associated with neuronal function were nDEGs (Figure 1E). For example, the expression of genes involved in dendrite development, such as reelin (*RELN*), leukocyte-specific transcript 1 (*LST1*), and Ephrin A1 (*EFNA1*), crucial for synaptic regulation,[21–23] remained unchanged. Similarly, key genes implicated in neuronal apoptosis, such as mitogen-activated protein kinase 7 (*MAP2K7*), beta-secretase 1 (*BACE1*), and sirtuin 1 (*SIRT1*), were not differentially expressed during AD progression.[24–27] The expression of additional genes, including cool-interacting tyrosine-phosphorylated protein 2 (*GIT2*), metallothionein 3 (*MT3*), obscurin such as cytoskeletal adaptor 1 (*OBSL1*), abelson tyrosine-protein kinase 1 (*ABL1*), endosome-associated trafficking regulator 1 (*ENTR1*), and histone deacetylase 6 (*HDAC6*), which are involved in various aspects of neuronal and nervous system regulation by modulating ion conduction, membrane, and microtubule functions, also remained stable (Figures 1F and S1A).[28–31]

While pathways enriched in DEGs aligned with recognized aspects of AD pathology, a notable finding was the considerable functional overlap between nDEGs and DEGs: Nearly 80% of DEG-enriched pathways were also represented among the nDEGs. These results suggest that nDEGs may contribute to AD pathology.

AS events in AD

Numerous genes associated with neuronal function do not exhibit changes in expression, some of which are critical to AD development. Thus, we investigated how these nDEGs influence AD progression. Notably, we identified 969 nDEGs whose transcript isoforms exhibited significant expression differences (defined by $|dIF| > 0.1$ and p-value < 0.05; Figures 1G and 1H, and Tables S2, S3, and S4).

Such variation in transcript usage often results from mechanisms such as AS or modifications at transcript start or end sites. To specifically assess AS, we used rMATS to exclude genes where isoform differences were due solely to initiation or termination shifts, resulting in 938 genes primarily characterized by AS events. From these, we identified 840 genes with significant differences in transcript isoform usage (Figure 2A; Tables S5 and S6), suggesting that AS events were responsible for generating the differentially expressed transcripts and the diversity of transcripts within nDEGs related to AD severity.

AS allows each gene to produce multiple transcript variants. Among the transcripts from the differentially spliced genes, only 892 underwent nonsense-mediated decay (NMD)—a process that eliminates mRNAs with premature stop codons (Figures 2B and S1B). Notably, ~29% of NMD-affected transcripts exhibited significant differences between AD and non-AD samples ($|dIF| > 0.1$, p-value <0.05; Figure S1B). Given that NMD can halt or eliminate protein production in non-coding transcripts, we excluded these complex, non-protein-coding transcripts from further analysis (Figures 2B and S1B).

Subsequently, we employed Metascape to analyze the biological pathways associated with the parental genes of the remaining transcripts. The findings revealed robust enrichment in inflammatory processes and AD-related pathways, highlighting the potential involvement of AS-derived nDEGs transcripts in AD pathology (Figure 2C).

AS pattern in AD

AS encompasses five main types: exon skipping (ES), alternative 3′ splice site selection (A3SS), alternative 5′ splice site selection (A5SS), intron retention (IR), and mutually exclusive exons (MXE; Figure 2D). Through AS, a single gene can produce myriad distinct transcripts, enabling various biological functions. Our comprehensive analysis of AS events in differential transcripts revealed ES as the predominant pattern (Figures 2E and 2F; Tables S7 and S8), aligning with previous studies.[32] After removing 42 non-coding or pseudogene-derived transcripts (5%), we identified 798 protein-coding transcripts (95%; Figure 2F and Table S9).

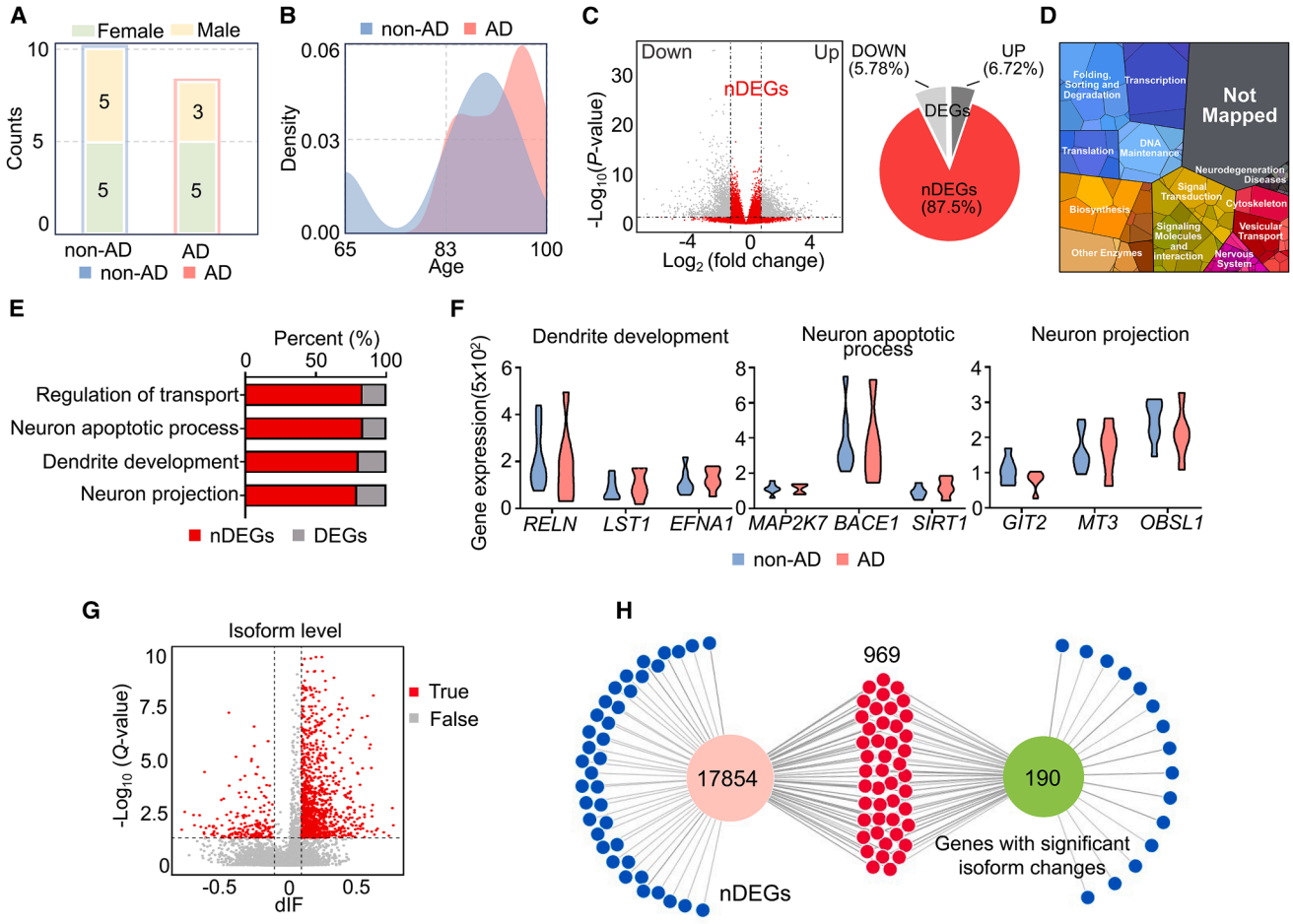

Figure 1. nDEGs analysis in patients with AD

(A and B) Bulk-RNAseq results in hippocampal tissues were collected from GSE173955, encompassing patients with AD (n = 8) and non-AD (n = 10) elderly individuals, with information on both age and sex included.

(C) A volcano plot depicts gene expression in GSE173955, with gray dots indicating differentially expressed genes (DEGs) and red dots representing nDEGs.

(D) Proteomaps analysis of nDEGs based on transcripts per million (TPM).

(E) The percentage of DEGs and nDEGs within shared pathways related to neuron function.

(F) Expression profiles of representative genes for nDEGs in dendrite development, neuron apoptotic process, and neuron projection among AD and non-AD groups.

(G) A volcano plot was used to illustrate changes in transcript isoform levels, where the difference in isoform fraction (dIF) represents the differential abundance of each transcript.

(H) A Venn diagram was used to compare genes with significant differential isoforms and nDEGs. Blue dots represent non-overlapping genes, whereas red dots indicate genes shared by both groups.

Often, multiple AS events and patterns occur within a single gene, yielding diverse transcripts from precursor mRNAs and resulting in the alteration or loss of protein-coding frames.[11] Most transcripts displayed more than one AS pattern and included multiple AS events, significantly impacting the genetic information within transcripts of the same gene and leading to diverse expression profiles (Figures 2G and 2H; Tables S10 and S11).

Considering that ES and MXE result in skipped or deleted exons, we examined the percentage of spliced-in (PSI) changes for transcripts with ES and MXE events in AD compared to non-AD conditions. Genes associated with ES transcripts were predominantly enriched in neuronal and nervous system functions (Figures 2I and 2J; Tables S12 and S14), whereas those with MXE events were associated with cellular structural functions, with some involvement in neuronal and synaptic functions (Figures 2K and 2L; Tables S13 and S15).

Cumulatively, these findings suggest that loss of genetic information due to AS events, particularly ES and MXE, may influence nervous system functions and potentially contribute to AD pathogenesis.

Dominant transcript isoform switching in AD conditions

The biological function underlying transcript isoform dynamics is complex, as evidenced by the diverse expression profiles observed in high-throughput RNA sequencing data. For

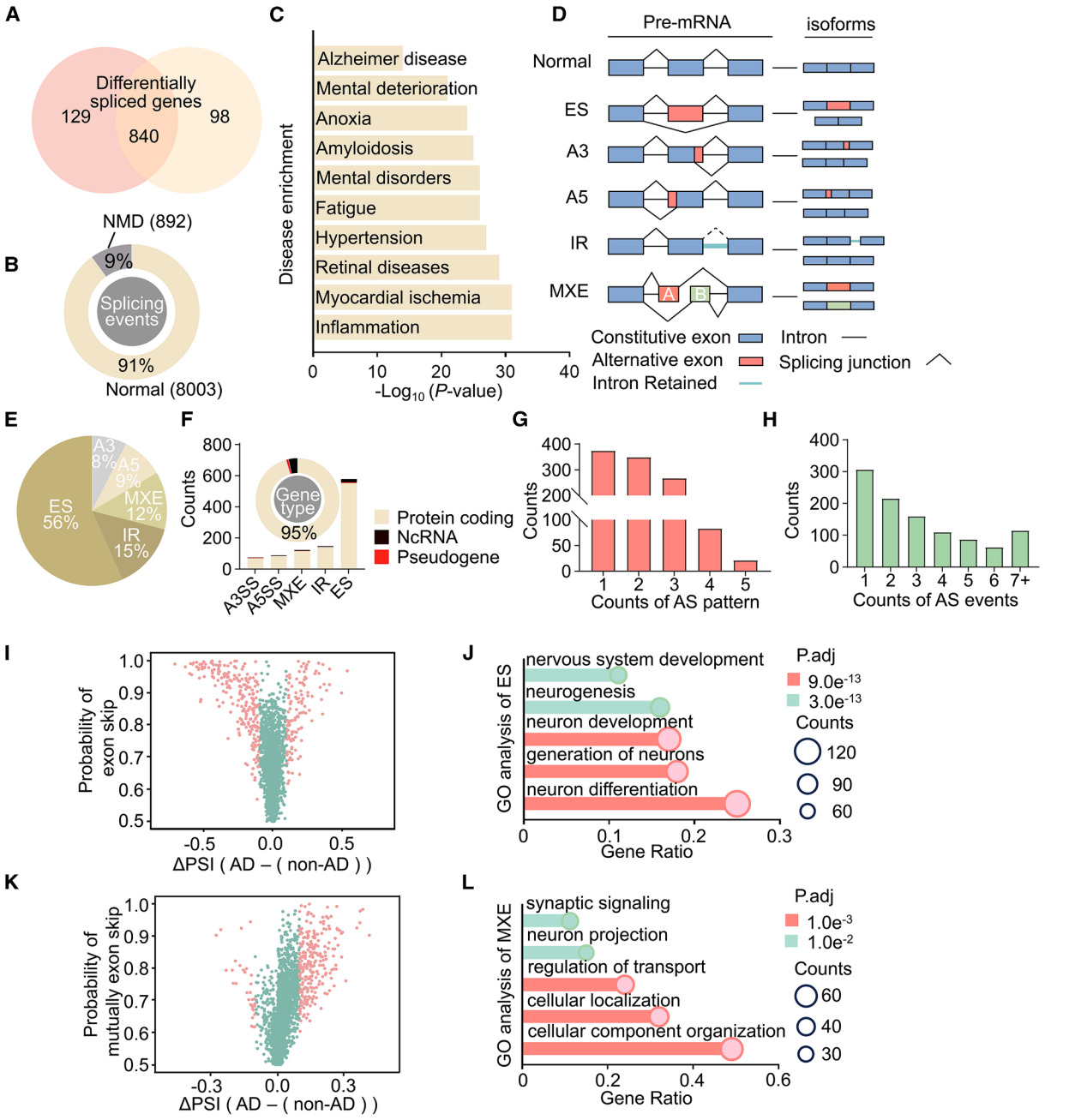

Figure 2. Changes in AS events in AD pathological conditions

(A) Differentially spliced genes were identified through a Venn diagram by overlapping genes with altered transcript isoform usage and nDEGs with genes exhibiting significant AS events.

(B) Percentage of transcripts undergoing NMD among AS event transcripts in differentially spliced genes.

(C) Disease enrichment analysis of differentially spliced genes using Metascape analysis.

(D) Splicing patterns of AS events.

(E) Proportion of different AS patterns among differentially spliced genes' transcripts excluded NMD.

(F) Bar and pie charts illustrate the numbers of different splicing events and the corresponding gene types in which these splicing events occur.

(G and H) Numbers of AS patterns and AS events in each gene, respectively.

(I and J) Volcano plot and gene function enrichment meteor plot of differentially expressed ES events between AD and non-AD.

(K and L) Volcano plot and gene function enrichment meteor plot of differentially expressed MXE events between AD and non-AD.

analytical clarity, we defined transcripts originating from a single gene as serving equivalent functional roles and focused our research on overall gene expression levels. While this approach facilitated characterization of genes with altered expression under physiological and pathological conditions, it overlooked the contributions of genes without expression changes and neglected the intricacies of AS patterns and events (Figures 2G and 2H).

Precursor mRNA splicing involves intricate exon selection—either inclusion or exclusion—that produces distinct transcript variants containing unique genetic information. The predominant variant is designated the major isoform, and variations in its dominance across different physiological states are referred to as isoform switching. This phenomenon represents a shift in the dominant isoform, which preserves total transcript abundance yet potentially alters protein function (Figure 3A).

Isoform switching may alter protein-coding sequences by modifying open reading frames (ORFs) through changes in exon usage that affect start and stop codons. Thus, AS can generate an expanded repertoire of genetic variants, leading to differential protein products from the same gene under different pathological conditions (Figure S1C).

To elucidate isoform-switch dynamics and their functional consequences, we used the IsoformSwitchAnalyzeR package to identify isoform-switch events and their associated outcomes. Among differentially spliced genes, we identified 642 that showed isoform switches between the non-AD and AD cohorts (Figure 3B and Table S16). Notably, isoform switches were evident in genes related to membrane transport (G-protein signaling modulator 2 [*GPSM2*], *d*ispatched RND transporter family member 1 [*DISP1*]), protein-protein interactions (N-recognin [*UBR1*], leucine-rich melanocyte differentiation-associated protein isoform 1 [*LRMDA*]), and enzymatic activity (mannosidase alpha class 2a member 2 [*MAN2A2*], galactokinase 1 [*GALK1*]; Figure 3C).

Analysis of isoform-switch consequences showed that the most dominant transcripts under AD conditions possessed extended ORFs and additional domains, indicative of increased genetic content (Figure 3D and Table S17). A greater proportion of non-coding transcripts also suggests cellular adaptation to AD-associated pathology within the hippocampus (Figure 3D). The assessment of coding potential further revealed that most variant transcripts were capable of coding (Figure 3E and Table S18).

Functional enrichment analysis of coding transcripts demonstrated involvement in processes, such as microtubule organizing center, Golgi membrane structure, and commissural neuron axon guidance, with notable differences in transcript usage for genes such as neural cell adhesion molecule 1 (*NCAM1*), vacuolar protein sorting-associated protein 72 homolog (*VPS72*), and G-protein-coupled receptor kinase-interacting protein 1 (*GIT1*; Figures 3F and S1D)—all established contributors to neurodegenerative diseases.[28,33–36]

Comparison of domain coding among transcripts affected by AD-induced isoform switches revealed that the transcription factor cysteine-2 histidine-2 (zf-C2H2) zinc finger domain accounted for a prominent proportion of these genes. This suggested that AS events may critically influence AD pathogenesis by modulating transcription factors.[37,38] Additionally, the enrichment of WD40, PDZ, and LIM domains suggests potential alterations in signaling pathways, including those involving ion channels and membrane-related functions, during AD progression (Figure S1E).[39–41]

Screening of spliced candidate genes in AD

To simplify the analysis of gene transcripts, we focused on genes with two transcripts that were significantly differentially expressed between the AD and non-AD groups, ultimately identifying 155 genes with fewer than three transcripts (Figures 3G and S2A). After removing non-coding transcripts, 36 genes remained, each with two protein-coding transcripts (Figures 3G and S2A).

Furthermore, only 36 genes possessed two primary transcripts that were both protein-coding (Figures 3G and S2A). We then analyzed the resulting proteins and coding sequences from isoform switching and highlighted the 15 genes with the largest predicted peptide sequence divergence, including Jade family PHD finger 1 (*JADE1*), round spermatid basic protein 1-like (*RSBN1L*), and Pleckstrin homology domain-containing family member 7 (*PLEKHA7*; Figure 3H).

NCAM1 AS event in AD

Given that RNA splicing is prevalent under physiological and pathological conditions, it is expected to occur during AD in mice. Analysis of 15 genes in murine models demonstrated that their two transcript variants shared high sequence similarities (>95%) with human orthologs, including neural cell adhesion molecule 1 (*NCAM1*), glycoprotein M6B (*GPM6B*), and bridging integrator 1 (*BIN1*) (Figures 4A and S3A).

Due to the highest degree of homology between human and mouse *NCAM1,* subsequent analysis focused on *NCAM1*, a cell adhesion protein integral to neurogenesis, neurite outgrowth, and cell migration during nervous system development (Table S19). Two primary *NCAM1* isoforms were identified in humans—L-*NCAM1* (long) and S-*NCAM1* (short)—with no significant difference in overall *NCAM1* expression observed between AD and non-AD groups (Figure 4B; Tables S20 and S21), as determined by an absolute value of log2 fold change below 1, consistent with established transcriptomic thresholds for biological significance.[42]

Notably, in patients with AD, the upregulation of S-*NCAM1* and downregulation of L-*NCAM1* were evident. Isoform-specific analyses using unpaired two-tailed *t*-tests with Benjamini-Hochberg FDR correction revealed significant differences: $p = 3.75 \times 10^{-4}$ for L-*NCAM1* and $p = 2.0 \times 10^{-6}$ for S-*NCAM1*; for isoform fraction, both yielded $p = 1.0 \times 10^{-6}$ (Figure 4B). Structural examination indicated loss of exons 9, 18, 19, and 20, as well as the insertion of a unique exon (representing the intronic region between exons 17 and 18) in S-*NCAM1* (Figures 4B and 4C).[35,43,44]

Considering that NCAM1 functions as a transmembrane protein involved in nervous system development,[35,43,44] we analyzed the transmembrane topology and intracellular domain structure of the two *NCAM1* transcripts using DeepTMHMM.[45] Although both transcripts exhibited similar

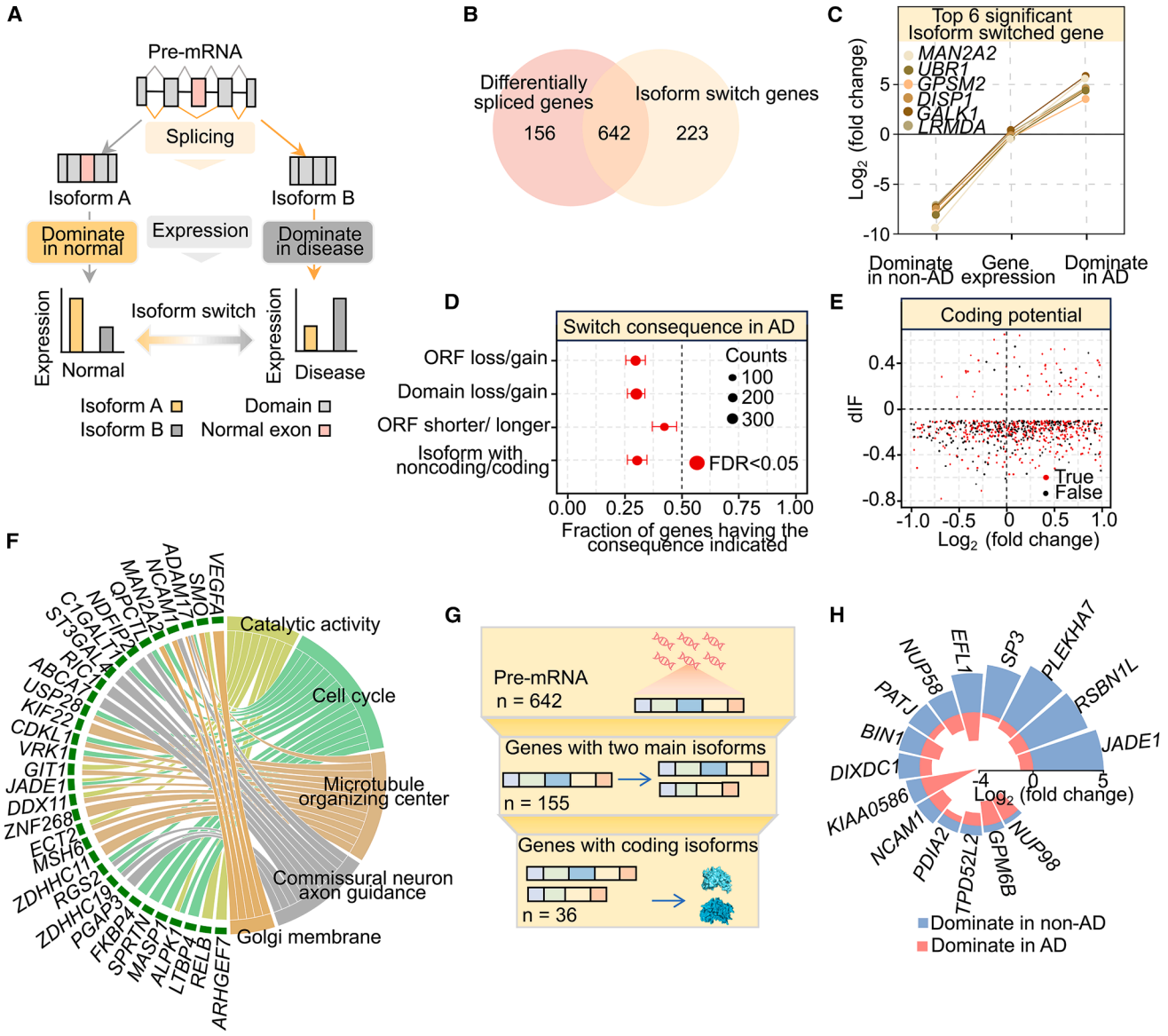

Figure 3. AS-caused isoform switch in AD conditions

(A) Precursor message RNA (pre-mRNA) generates different transcripts through different splicing patterns.

(B) A Venn diagram showing genes in which splicing events generate differentially expressed transcripts and are also characterized by an isoform switch.

(C) Among the isoform-switched genes, the isoform transcripts were switched in AD conditions, reflecting in the difference of dominate isoforms between non-AD and AD.

(D) Different consequences resulting from isoform switch in AD and non-AD. The proportion of genes is presented with different switch consequences.

(E) The coding potential for 642 isoform switch genes. The difference in predominant transcripts between the AD and non-AD is calculated by dIF.

(F) Functional analysis of these genes is presented, showing that they are related to the Golgi membrane, the microtubule-organizing center, and catalytic activity.

(G and H) The brief outflow for 642 genes is performed for further screening, and 15 genes are left. And their expression profile is presented both in non-AD and AD conditions.

extracellular domains, including multiple immunoglobulin family domains and Fn domains, the intracellular domain was absent from S-*NCAM1*, in contrast to the full-length L-*NCAM1* (Figures 4C, 4D, and S3B). AlphaFold3 prediction further demonstrated that the deletion of exons 18–20 in S-*NCAM1* significantly altered the protein's C-terminal structure and consequently its transmembrane topology (Figure S3C).[46]

To confirm the presence of AS events in *NCAM1* under AD conditions, rmats analysis was performed, detecting two AS sites: exon 9 skipping in S-*NCAM1* and a unique insertion instead of exons 18–20 (Figure 4E). These findings suggest that S-*NCAM1* serves as a transcript marker for AD pathology, while L-*NCAM1* predominates in non-AD individuals, reflecting an isoform switch associated with the disease state.

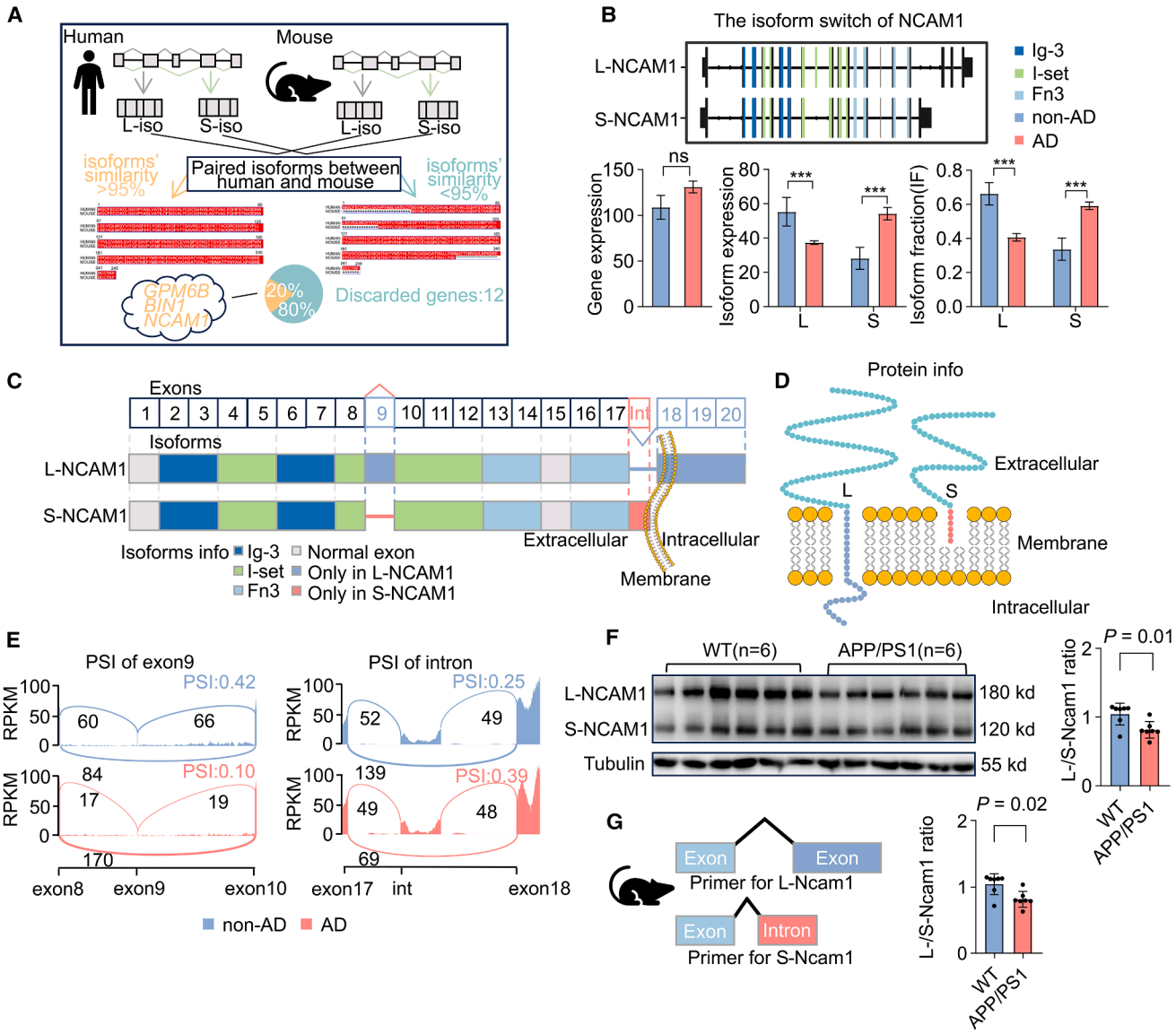

Figure 4. *NCAM1* AS events in AD conditions

(A) Screening for homologous genes with similar transcripts between humans and mice. By pairing the L-iso and S-iso forms in humans with their counterparts in mice and comparing their similarity with a cutoff value of 95%.

(B) Genomic information of NCAM1 transcripts and protein domains. The transcriptional levels of NCAM1 and the levels of NCAM1 isoforms in non-AD and AD conditions are shown. At the gene level, significant differential expression was defined as $|\log2FC| > 1$. Statistical significance was determined using a two-tailed unpaired Student's *t* test with Benjamini-Hochberg correction. $^{*}p < 0.05$, $^{**}p < 0.01$, and $^{***}p < 0.001$ (AD vs. non-AD).

(C) Exon details for these two transcripts of NCAM1.

(D) Membrane localization information for L-*NCAM1* and S-*NCAM1*.

(E) Identification of representative ES events for *NCAM1* and S-*NCAM1*. PSI (percent spliced in) reflects the usage of an exon, with a higher PSI value indicating increased exon usage. RPKM represents the abundance of the exon sequence.

(F) Western blot (WB) analysis was performed to detect the two isoforms of NCAM1 protein in the hippocampus of WT ($n = 6$) and APP/PS1 mice ($n = 6$). Representative immunoblots and densitometric quantification are shown. Statistical significance was assessed using an unpaired two-tailed Student's *t* test to obtain *p*-values.

(G) Isoform-specific primers were designed to distinguish L-Ncam1 and S-Ncam1 transcripts, and quantitative real-time PCR (qPCR) analysis was performed to assess the ratio of long to short Ncam1 transcript isoforms in the hippocampus of WT ($n = 10$) and APP/PS1 mice ($n = 10$). Statistical significance was assessed using an unpaired two-tailed Student's *t* test to obtain *p*-values.

Exon 9 skipping reduced L-*NCAM1* levels, whereas Intron skipping repressed S-*NCAM1* level; thus, exon 9 of *NCAM1* may serve as a specific non-AD marker, while the Int sequence is a tag for AD. Due to the presence of distinct 3′UTR regions, differential abundance was assessed using IGV analysis (Figure S3D). The S-*NCAM1* 3′UTR was significantly upregulated in patients with AD, whereas L-*NCAM1* exhibited the opposite trend, supporting substantial isoform-specific expression changes in AD pathogenesis (Figure S3D).

To substantiate these findings *in vivo*, we examined the expression of the two *Ncam1* isoforms in hippocampal tissues from six 6-month-old APP/PS1 mice and six age-matched controls (Figure S3E). Compared to controls, APP/PS1 mice exhibited a reduced L-NCAM1 (180 kDa) to S-NCAM1 (120 kDa) ratio, consistent with the altered AS of *Ncam1* (Figure 4F and Table S22). This confirms the dynamic transcript usage of *Ncam1* across different pathological states and underscores that genes with stable total expression may generate functionally diverse proteins via AS.

To further substantiate the identity of the *Ncam1* isoforms undergoing switching, RT-qPCR analysis was performed using total RNA extracted from hippocampal tissues of ten 6-month-old APP/PS1 mice and ten age-matched controls. Isoform-specific primers targeting S-*Ncam1* and L-*Ncam1* were used for the analysis (Figure 4G). Compared to controls, APP/PS1 mice exhibited a significantly reduced L-*Ncam1*/S-*Ncam*1 ratio, consistent with the western blot results (Figure 4G and Table S23). This confirms the occurrence of isoform switching of *Ncam1* in APP/PS1 mice and further identifies the specific *Ncam1* isoforms involved in this switching event.

The concordant shifts in *NCAM1*/*Ncam1* transcript utilization observed in human hippocampal tissues and mice suggest that this phenomenon is a general feature of AD pathology across species. This broadens our understanding of the molecular mechanisms underlying AD and highlights the complexity of AS-mediated transcriptomic regulation as an important contributor to disease progression, with potential relevance as a source of biomarkers or therapeutic strategies.

Isoform switch of *Ncam1* in astrocytes in AD

To confirm whether the AS events of *Ncam1* occur under AD conditions, we analyzed single-nucleus RNA sequencing data (GSE221959) from the hippocampus of 14-month-old AD-BXD mice (n = 6) and age-matched wild-type (WT) mice (n = 6). This facilitated the evaluation of cell-type-specific AS patterns and the *Ncam1* gene expression profile in the hippocampus (Figure 5A). Using quality control and unsupervised clustering, we observed the presence of alternative exons in each cell cluster, reflecting numerous differential splicing events across cell types (Figure S4A). Although the expression of most genes was constant across cell types under AD conditions compared to that under normal conditions, these genes underwent splicing with significant variation in exon usage, leading to isoform switching, consistent with the findings from the bulk RNA sequencing assay (Figure S4B). Notably, cell-specific splicing events predominantly emerged in endothelial cells, neurons, and astrocytes, with enrichment in genes involved in nitrogen compound metabolism, neural function, and development (Figures S4C and S4D; Tables S24, S25, S26, S27, S28, S29, and S30).

For the AS event of *Ncam1,* we observed robust total *Ncam1* expression in neurons, oligodendrocytes, oligodendrocyte precursor cells, and astrocytes under physiological and pathological conditions (Figures 5B and 5C; Table S31). Given the specificity of the unique Int exon in S-*Ncam1*, we utilized Int expression as a marker for S-*Ncam1* to detect spliced transcripts under AD conditions (Figure 4C). Notably, S-*Ncam1* Int exon expression was predominantly observed in astrocytes, with a significantly higher PSI value in the AD group than in the non-AD group. This suggested that astrocytes in the hippocampus were the primary site for differential S-*Ncam1* expression under AD pathological conditions (Figures 5D and 5E; Table S32).

Given that *Ncam1* splicing predominantly occurred in astrocytes, we examined the relationship between S-*Ncam1* levels and AD severity in these cells. Three distinct subgroups of astrocytes were detected: homeostatic state (Ast1; expressing *Slc7a10* and *Luzp2*), transitional state (Ast2; expressing *Mfge8*), and activated state (Ast3 expressing *Ctsb* and *Gfap*) (Figures 5F, S4E, and S4F).[47] Analysis revealed that Ast3 astrocytes displayed the highest relative expression of S-*Ncam*1 and the greatest PSI value (S-*Ncam*1/Total-*Ncam*1) (Figures 5G and 5H), indicating enhanced *S-Nca*m1 expression in activated astrocytes. The upregulation of *S-Nca*m1 in activated astrocytes within AD models suggests that loss of the intracellular domain of NCAM1 may affect astrocytic function and potentially modulate their response to AD pathology.[48]

DISCUSSION

This study identified a phenomenon in which many genes with stable overall expression levels exhibited substantial transcriptional isoform switching during AD progression. These findings underscore the potential role of AS in AD pathogenesis. Analysis of AS patterns in hippocampal tissues from patients with AD compared to non-AD controls revealed that these events were associated with disease severity. Specifically, *NCAM1* emerged as a key gene affected by AS in AD. As AD pathology progresses, AS of NCAM1 transitions from L-NCAM1 to S-NCAM1, potentially resulting in the loss of NCAM1's intracellular domain and subsequent partial functional impairment. These findings contribute to a deeper understanding of the molecular mechanisms underlying AD development and suggest that isoform switching may represent a marker of AD, with implications for its use as a potential biomarker.

Recent studies on AS in AD have primarily used animal models. For instance, Lu et al. examined the AS profile in the cerebral cortex of 9-month-old APP/PS1 mice and in hippocampal microglia from both APP and non-transgenic (Ntg) mice.[49,50] However, many mouse models of AD, including Tg2576, TgCRND8, APP/PS1, 5×FAD, and 3×Tg-AD, fail to replicate certain clinical features of AD.[51,52] For example, the 3×Tg model does not develop neuronal loss, even in the presence of Aβ deposits and tau pathology.

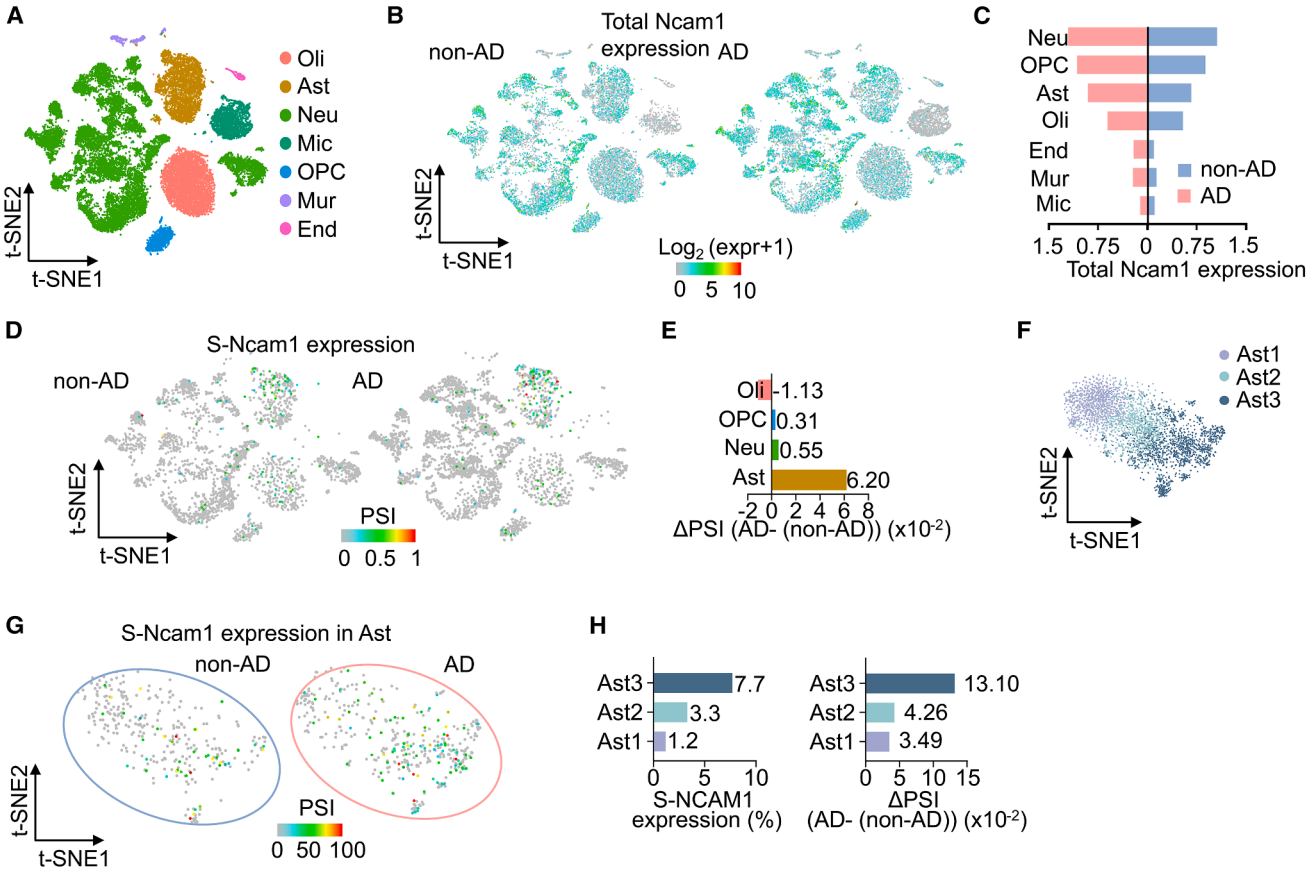

Figure 5. AS event of *Ncam1* in astrocytes following AD

(A) Single-nucleus RNA sequencing (snRNA-seq) data from hippocampal tissues of WT (n = 6) and 14-month-old AD-BXD (n = 6) mice were analyzed using t-distributed stochastic neighbor embedding (t-SNE) for unsupervised clustering. Cell-type annotations are indicated as follows: Oli, oligodendrocytes; Ast, astrocytes; Neu, neurons; Mic, microglia; OPC, oligodendrocyte progenitor cells; Mur, mural cells; End, endothelial cells.

(B) Expression of total Ncam1 in various cell populations in the mouse hippocampus under different pathological conditions. Each dot represents a cell, and the color of the dot represents the expression level, with darker colors indicating higher expression.

(C) Total-Ncam1 expression levels in different cells in the hippocampus.

(D) S-Ncam1 expression levels in various cell populations.

(E) Difference of S-Ncam1 to total-Ncam1 in the different cell populations following AD.

(F) Subclassification of astrocyte subpopulations, dividing astrocytes into Ast1, Ast2, and Ast3.

(G) The expression level of S-Ncam1 in different types of astrocytes.

(H) Portion of S-Ncam1 in total Ncam1 in different astrocytes. And the differences in the usage of Int sequence among various astrocyte subpopulations under different pathological conditions.

In the current study, we analyzed RNA sequencing data from hippocampal tissues of patients with AD and a non-AD cohort to gain detailed insights into expression patterns and subtle changes across AD progression in real-world clinical settings. Given that splicing significantly contributes to transcriptome diversity, we identified numerous genes exhibiting splicing events during AD progression, particularly those with functions related to the microtubule organizing center, the Golgi membrane, and axon guidance of commissural neurons—all of which are associated with AD severity. Among these, the long isoform of *NCAM1* (L-*NCAM1*) is the predominant transcript in the hippocampus under normal conditions; however, under AD conditions, there is a shift toward the short isoform, leading to a marked decrease in the L-*NCAM1*-to-S-*NCAM1* ratio. This alteration was also more evident in APP/PS1 AD mice than in WT mice (Figure 4F).

AS of primary transcripts is a complex process that significantly influences various pathological conditions. Many genes undergo multiple splicing events, particularly in AD.[53] The NCAM1 gene, for instance, features two distinct splicing events associated with AD. The first involves the deletion of exon 9 in the L-NCAM1 variant, while the second is more elaborate—entailing the loss of exons 18, 19, and 20, along with the incorporation of an intron-derived exon between *exons* 17 and 18 in the S-NCAM1 transcript during AD. These splicing events occur at different sites within the *NCAM1* pre-mRNA, resulting in the production of S-*NCAM1*, which lacks an intracellular domain.

The *NCAM1* gene is evolutionarily conserved and plays a crucial role in learning and memory, as well as in various brain-related biological processes, including synaptic plasticity, neuronal migration, axonal branching, fasciculation, and synaptogenesis.[54] The absence of an intracellular domain in S-NCAM1 disrupts the signal transduction pathway from the extracellular to the intracellular membrane, indicating that NCAM1's biological function may be altered under these circumstances—a change with potentially significant impacts on neuronal communication in AD.

AS events involving *NCAM1* predominantly occur in astrocytes. While bulk RNA sequencing provides the landscape of splicing events in hippocampal tissues from patients with AD, single-nucleus sequencing offers a deeper look into cell-type complexity by creating a comprehensive atlas of human brain cells. Combining single-nucleus and bulk sequencing provides more detailed insights into splicing events in AD. AS events reportedly manifest in various cell types within the prefrontal cortex of AD brains, affecting the splicing and expression of transcripts linked to chaperones, such as heat shock protein 90 alpha family class A member 1 (*HSP90AA1*) in microglia and neurons with tauopathy, prostaglandin D2 synthase (*PTGDS*) in astrocytes and endothelial cells, and transient receptor potential melastatin 2 (*TRPM2*) in astrocytes and excitatory neurons.[55]

Our investigation of hippocampal tissues indicates that the switch from L-*NCAM1* to S-*NCAM1* predominantly occurred in astrocytes under AD conditions, not in other astrocyte subtypes. Reactive astrocytes remodel their morphology, molecular structure, and function in response to injury, illness, or infection.[56] Thus, the transcriptional shift to S-NCAM1 and loss of the intracellular domain disrupts the original function of NCAM1 in astrocytes.[56]

However, the role of altered NCAM1 expression throughout the progression of AD pathology was not fully elucidated in this study. Attempts to knock down S-NCAM1 levels in Aβ-induced SVG-p12 astrocyte models using siRNA targeting S-NCAM1 did not yield notable phenotypic changes. This suggests that physiological levels of S-NCAM1 play an essential role in maintaining astrocyte function under AD conditions, and abnormally low S-NCAM1 levels may contribute to AD onset. Moreover, efforts to restore the intracellular function of NCAM1 via L-NCAM1 overexpression were impacted by competitive interactions between exogenous and endogenous proteins, as reported in previous studies.[57,58] Even with increased exogenous L-NCAM1, robust competition from endogenous S-NCAM1 precluded rescue of effects attributable to S-NCAM1.

Nevertheless, AS-generated isoforms offer expanded opportunities for investigating genes without significant expression changes. Our findings underscore the relevance of genes that are not differentially expressed. Notably, after a series of screening tests, we identified *NCAM1* as a key gene.

Limitations of the study

This study has some limitations. Due to stringent regulations surrounding human brain datasets, we could not obtain permission for their use and consequently relied on publicly available data from the Gene Expression Omnibus database. Unfortunately, accessible sample information was limited to age and sex, and the sample size included only 18 individuals. This constraint raises concerns regarding the reliability of our analyses.

In the next phase of research, we aim to enhance the accuracy and generalizability of key gene identification by leveraging rigorously curated databases, such as ROSMAP and MSBB. This approach will increase our sample size and facilitate the acquisition of detailed AD-specific information, including measures such as MMSE, CERAD, and Braak scores. This will significantly enhance the reliability and representativeness of the results. Using these data, we will create a comprehensive differential AS map based on nDEGs, combining multiple indicators to thoroughly depict the evolution of AS during the pathological process of AD, thereby deepening our understanding of the molecular mechanisms of AD.

Regarding NCAM1, challenges remain in delineating its various isoforms and assessing their functional loss within the context of AD pathology. Nevertheless, elucidating the roles and mechanisms of NCAM1—particularly L-NCAM1 and S-NCAM1—in both non-AD and AD-affected brains, as well as investigating alterations in splicing factors contributing to isoform differences, will offer insights and directions for unraveling the complexities of AD pathogenesis.

RESOURCE AVAILABILITY

Lead contact

Requests for further information and resources should be directed to and will be fulfilled by the lead contact, Qiulun Lu (qiulunlu@cpu.edu.cn).

Materials availability

Materials generated in this study will be made available as allowed by China Pharmaceutical University policy.

Data and code availability

- This study analyzes publicly available data accessible through the NCBI Gene Expression Omnibus, and the details of the analyzed datasets are provided in the key resources table.
- This paper does not report original code.
- The processed data generated in this study are available in the supplementary materials. Any additional information required to reanalyze the data reported in this paper is available from the lead contact upon request.

ACKNOWLEDGMENTS

This study was supported by the grants from the Leading Technology Foundation Research Project of Jiangsu Province (BK20192005), Sanming Project of Medicine in Shenzhen (SZSM201801060), The China Postdoctoral Science Foundation (2024T171037), the Natural Science Foundation of Jiangsu Province (BK20221051), and the Postdoctoral Excellence Program of Jiangsu Province (2022ZB297). Author disclosures are available in the supporting information.

AUTHOR CONTRIBUTIONS

H.L. and S.L. performed the bioinformatics analysis and data processing. D.M. was responsible for figure preparation. L.C. and Y.S. conducted the animal experiments. Q.L. conceived the study and drafted the manuscript. G.W., Z.Z., and X.L. provided critical revision of the manuscript. All authors reviewed and approved the final version of the manuscript.

DECLARATION OF INTERESTS

The authors declare no conflicts of interest.

STAR★METHODS

Detailed methods are provided in the online version of this paper and include the following:

- KEY RESOURCES TABLE
- EXPERIMENTAL MODEL AND STUDY PARTICIPANT DETAILS
  - AD mouse model
- METHOD DETAILS
  - Transcriptome assembly and quantification from RNA-seq data
  - Analysis of AS events
  - Functional enrichment analysis
  - Isoform switching analysis
  - Single nucleus RNA sequencing analysis
  - Western blot assay
  - RNA isolation and RT–qPCR analysis
- QUANTIFICATION AND STATISTICAL ANALYSIS

SUPPLEMENTAL INFORMATION

Supplemental information can be found online at https://doi.org/10.1016/j.isci.2026.115456.

Received: September 15, 2025
Revised: December 19, 2025
Accepted: March 19, 2026
Published: March 26, 2026

REFERENCES

1. Barker, W.W., Luis, C.A., Kashuba, A., Luis, M., Harwood, D.G., Loewenstein, D., Waters, C., Jimison, P., Shepherd, E., Sevush, S., et al. (2002). Relative frequencies of Alzheimer disease, Lewy body, vascular and frontotemporal dementia, and hippocampal sclerosis in the State of Florida Brain Bank. Alzheimer Dis. Assoc. Disord. *16*, 203–212. https://doi.org/10.1097/00002093-200210000-00001.
2. Winblad, B., Amouyel, P., Andrieu, S., Ballard, C., Brayne, C., Brodaty, H., Cedazo-Minguez, A., Dubois, B., Edvardsson, D., Feldman, H., et al. (2016). Defeating Alzheimer's disease and other dementias: a priority for European science and society. Lancet Neurol. *15*, 455–532. https://doi.org/10.1016/S1474-4422(16)00062-4.
3. Rosenberg, R.N., Lambracht-Washington, D., Yu, G., and Xia, W. (2016). Genomics of Alzheimer Disease: A Review. JAMA Neurol. *73*, 867–874. https://doi.org/10.1001/jamaneurol.2016.0301.
4. Knopman, D.S., Amieva, H., Petersen, R.C., Chételat, G., Holtzman, D.M., Hyman, B.T., Nixon, R.A., and Jones, D.T. (2021). Alzheimer disease. Nat. Rev. Dis. Primers *7*, 33. https://doi.org/10.1038/s41572-021-00269-y.
5. Nik, S., and Bowman, T.V. (2019). Splicing and neurodegeneration: Insights and mechanisms. Wiley Interdiscip. Rev. RNA *10*, e1532. https://doi.org/10.1002/wrna.1532.
6. van Rooij, J.G.J., Meeter, L.H.H., Melhem, S., Nijholt, D.A.T., Wong, T.H., Netherlands Brain Bank; Rozemuller, A., Uitterlinden, A.G., van Meurs, J.G., and van Swieten, J.C. (2019). Hippocampal transcriptome profiling combined with protein-protein interaction analysis elucidates Alzheimer's disease pathways and genes. Neurobiol. Aging *74*, 225–233. https://doi.org/10.1016/j.neurobiolaging.2018.10.023.
7. Klyucherev, T.O., Olszewski, P., Shalimova, A.A., Chubarev, V.N., Tarasov, V.V., Attwood, M.M., Syvänen, S., and Schiöth, H.B. (2022). Advances in the development of new biomarkers for Alzheimer's disease. Transl. Neurodegener. *11*, 25. https://doi.org/10.1186/s40035-022-00296-z.
8. Kim, S., Chun, H., Kim, Y., Kim, Y., Park, U., Chu, J., Bhalla, M., Choi, S.-H., Yousefian-Jazi, A., Kim, S., et al. (2024). Astrocytic autophagy plasticity modulates Aβ clearance and cognitive function in Alzheimer's disease. Mol. Neurodegener. *19*, 55. https://doi.org/10.1186/s13024-024-00740-w.
9. Quiroz, Y.T., Aguillon, D., Aguirre-Acevedo, D.C., Vasquez, D., Zuluaga, Y., Baena, A.Y., Madrigal, L., Hincapié, L., Sanchez, J.S., Langella, S., et al. (2024). APOE3 Christchurch Heterozygosity and Autosomal Dominant Alzheimer's Disease. N. Engl. J. Med. *390*, 2156–2164. https://doi.org/10.1056/NEJMoa2308583.
10. Agatemor, C., Middleton, S.A.D., and Toledo, D. (2022). How pervasive are post-translational and -transcriptional modifications? Trends Cell Biol. *32*, 475–478. https://doi.org/10.1016/j.tcb.2021.11.002.
11. Marasco, L.E., and Kornblihtt, A.R. (2023). The physiology of alternative splicing. Nat. Rev. Mol. Cell Biol. *24*, 242–254. https://doi.org/10.1038/s41580-022-00545-z.
12. Baralle, F.E., and Giudice, J. (2017). Alternative splicing as a regulator of development and tissue identity. Nat. Rev. Mol. Cell Biol. *18*, 437–451. https://doi.org/10.1038/nrm.2017.27.
13. Wright, C.J., Smith, C.W.J., and Jiggins, C.D. (2022). Alternative splicing as a source of phenotypic diversity. Nat. Rev. Genet. *23*, 697–710. https://doi.org/10.1038/s41576-022-00514-4.
14. Tao, Y., Zhang, Q., Wang, H., Yang, X., and Mu, H. (2024). Alternative splicing and related RNA binding proteins in human health and disease. Signal Transduct. Target. Ther. *9*, 26. https://doi.org/10.1038/s41392-024-01734-2.
15. Raj, T., Li, Y.I., Wong, G., Humphrey, J., Wang, M., Ramdhani, S., Wang, Y.-C., Ng, B., Gupta, I., Haroutunian, V., et al. (2018). Integrative transcriptome analyses of the aging brain implicate altered splicing in Alzheimer's disease susceptibility. Nat. Genet. *50*, 1584–1592. https://doi.org/10.1038/s41588-018-0238-1.
16. Buchholz, S., and Zempel, H. (2024). The six brain-specific TAU isoforms and their role in Alzheimer's disease and related neurodegenerative dementia syndromes. Alzheimer's Dement. *20*, 3606–3628. https://doi.org/10.1002/alz.13784.
17. Lambert, E., Saha, O., Soares Landeira, B., Melo de Farias, A.R., Hermant, X., Carrier, A., Pelletier, A., Gadaut, J., Davoine, L., Dupont, C., et al. (2022). The Alzheimer susceptibility gene BIN1 induces isoform-dependent neurotoxicity through early endosome defects. Acta Neuropathol. Commun. *10*, 4. https://doi.org/10.1186/s40478-021-01285-5.
18. Zhang, D.-F., Fan, Y., Xu, M., Wang, G., Wang, D., Li, J., Kong, L.-L., Zhou, H., Luo, R., Bi, R., et al. (2019). Complement C7 is a novel risk gene for Alzheimer's disease in Han Chinese. Natl. Sci. Rev. *6*, 257–274. https://doi.org/10.1093/nsr/nwy127.
19. Xu, M., Zhang, D.-F., Luo, R., Wu, Y., Zhou, H., Kong, L.-L., Bi, R., and Yao, Y.-G. (2018). A systematic integrated analysis of brain expression profiles reveals YAP1 and other prioritized hub genes as important upstream regulators in Alzheimer's disease. Alzheimer's Dement. *14*, 215–229. https://doi.org/10.1016/j.jalz.2017.08.012.
20. Mizuno, Y., Abolhassani, N., Mazzei, G., Sakumi, K., Saito, T., Saido, T.C., Ninomiya, T., Iwaki, T., Yamasaki, R., Kira, J.-I., and Nakabeppu, Y. (2021). MUTYH Actively Contributes to Microglial Activation and Impaired Neurogenesis in the Pathogenesis of Alzheimer's Disease. Oxid. Med. Cell. Longev. *2021*, 8635088. https://doi.org/10.1155/2021/8635088.
21. Lopera, F., Marino, C., Chandrahas, A.S., O'Hare, M., Villalba-Moreno, N.D., Aguillon, D., Baena, A., Sanchez, J.S., Vila-Castelar, C., Ramirez Gomez, L., et al. (2023). Resilience to autosomal dominant Alzheimer's disease in a Reelin-COLBOS heterozygous man. Nat. Med. *29*, 1243–1252. https://doi.org/10.1038/s41591-023-02318-3.
22. Kim, J.P., Kim, B.-H., Bice, P.J., Seo, S.W., Bennett, D.A., Saykin, A.J., and Nho, K. (2023). Integrative Co-methylation Network Analysis Identifies Novel DNA Methylation Signatures and Their Target Genes in Alzheimer's Disease. Biol. Psychiatry *93*, 842–851. https://doi.org/10.1016/j.biopsych.2022.06.020.
23. Guan, L., Wang, Q., Wang, L., Wu, B., Chen, Y., Liu, F., Ye, F., Zhang, T., Li, K., Yan, B., et al. (2016). Common variants on 17q25 and gene-gene interactions conferring risk of schizophrenia in Han Chinese population and regulating gene expressions in human brain. Mol. Psychiatry *21*, 1244–1250. https://doi.org/10.1038/mp.2015.204.

24. Hadar, A., Kapitansky, O., Ganaiem, M., Sragovich, S., Lobyntseva, A., Giladi, E., Yeheskel, A., Avitan, A., Vatine, G.D., Gurwitz, D., et al. (2021). Introducing ADNP and SIRT1 as new partners regulating microtubules and histone methylation. Mol. Psychiatry *26*, 6550–6561. https://doi.org/10.1038/s41380-021-01143-9.

25. Ou-Yang, M.-H., Kurz, J.E., Nomura, T., Popovic, J., Rajapaksha, T.W., Dong, H., Contractor, A., Chetkovich, D.M., Tourtellotte, W.G., and Vassar, R. (2018). Axonal organization defects in the hippocampus of adult conditional BACE1 knockout mice. Sci. Transl. Med. *10*, eaao5620. https://doi.org/10.1126/scitranslmed.aao5620.

26. Müller, S.A., Shmueli, M.D., Feng, X., Tüshaus, J., Schumacher, N., Clark, R., Smith, B.E., Chi, A., Rose-John, S., Kennedy, M.E., and Lichtenthaler, S.F. (2023). The Alzheimer's disease-linked protease BACE1 modulates neuronal IL-6 signaling through shedding of the receptor gp130. Mol. Neurodegener. *18*, 13. https://doi.org/10.1186/s13024-023-00596-6.

27. Openshaw, R.L., Pratt, J.A., and Morris, B.J. (2022). The schizophrenia risk gene Map2k7 regulates responding in a novel contingency-shifting rodent touchscreen gambling task. Dis. Model. Mech. *15*, dmm049310. https://doi.org/10.1242/dmm.049310.

28. Montesinos, M.S., Dong, W., Goff, K., Das, B., Guerrero-Given, D., Schmalzigaug, R., Premont, R.T., Satterfield, R., Kamasawa, N., and Young, S.M. (2015). Presynaptic Deletion of GIT Proteins Results in Increased Synaptic Strength at a Mammalian Central Synapse. Neuron *88*, 918–925. https://doi.org/10.1016/j.neuron.2015.10.042.

29. Hebron, M.L., Lonskaya, I., and Moussa, C.E.H. (2013). Tyrosine kinase inhibition facilitates autophagic SNCA/α-synuclein clearance. Autophagy *9*, 1249–1250. https://doi.org/10.4161/auto.25368.

30. Yoshiyama, Y., Sato, H., Seiki, M., Shinagawa, A., Takahashi, M., and Yamada, T. (1998). Expression of the membrane-type 3 matrix metalloproteinase (MT3-MMP) in human brain tissues. Acta Neuropathol. *96*, 347–350. https://doi.org/10.1007/s004010050904.

31. Mondal, P., Bai, P., Gomm, A., Bakiasi, G., Lin, C.-C.J., Wang, Y., Choi, S.H., Tanzi, R.E., Wang, C., and Zhang, C. (2024). Structure-Based Discovery of A Small Molecule Inhibitor of Histone Deacetylase 6 (HDAC6) that Significantly Reduces Alzheimer's Disease Neuropathology. Adv. Sci. *11*, e2304545. https://doi.org/10.1002/advs.202304545.

32. Florea, L., Song, L., and Salzberg, S.L. (2013). Thousands of exon skipping events differentiate among splicing patterns in sixteen human tissues. F1000Res. *2*, 188. https://doi.org/10.12688/f1000research.2-188.v2.

33. Asmar, A.J., Abrams, S.R., Hsin, J., Collins, J.C., Yazejian, R.M., Wu, Y., Cho, J., Doyle, A.D., Cinthala, S., Simon, M., et al. (2023). A ubiquitin-based effector-to-inhibitor switch coordinates early brain, craniofacial, and skin development. Nat. Commun. *14*, 4499. https://doi.org/10.1038/s41467-023-40223-y.

34. Goehler, H., Lalowski, M., Stelzl, U., Waelter, S., Stroedicke, M., Worm, U., Droege, A., Lindenberg, K.S., Knoblich, M., Haenig, C., et al. (2004). A protein interaction network links GIT1, an enhancer of huntingtin aggregation, to Huntington's disease. Mol. Cell *15*, 853–865. https://doi.org/10.1016/j.molcel.2004.09.016.

35. You, Y., Muraoka, S., Jedrychowski, M.P., Hu, J., McQuade, A.K., Young-Pearse, T., Aslebagh, R., Shaffer, S.A., Gygi, S.P., Blurton-Jones, M., et al. (2022). Human neural cell type-specific extracellular vesicle proteome defines disease-related molecules associated with activated astrocytes in Alzheimer's disease brain. J. Extracell. Vesicles *11*, e12183. https://doi.org/10.1002/jev2.12183.

36. Cacciagli, P., Desvignes, J.-P., Girard, N., Delepine, M., Zelenika, D., Lathrop, M., Lévy, N., Ledbetter, D.H., Dobyns, W.B., and Villard, L. (2014). AP1S2 is mutated in X-linked Dandy-Walker malformation with intellectual disability, basal ganglia disease and seizures (Pettigrew syndrome). Eur. J. Hum. Genet. *22*, 363–368. https://doi.org/10.1038/ejhg.2013.135.

37. Wu, N.-Y., and Cheng, S.-C. (2019). Functional analysis of Cwc24 ZF-domain in 5' splice site selection. Nucleic Acids Res. *47*, 10327–10339. https://doi.org/10.1093/nar/gkz733.

38. Najafabadi, H.S., Mnaimneh, S., Schmitges, F.W., Garton, M., Lam, K.N., Yang, A., Albu, M., Weirauch, M.T., Radovani, E., Kim, P.M., et al. (2015). C2H2 zinc finger proteins greatly expand the human regulatory lexicon. Nat. Biotechnol. *33*, 555–562. https://doi.org/10.1038/nbt.3128.

39. Kim, E., and Sheng, M. (2004). PDZ domain proteins of synapses. Nat. Rev. Neurosci. *5*, 771–781. https://doi.org/10.1038/nrn1517.

40. Schapira, M., Tyers, M., Torrent, M., and Arrowsmith, C.H. (2017). WD40 repeat domain proteins: a novel target class? Nat. Rev. Drug Discov. *16*, 773–786. https://doi.org/10.1038/nrd.2017.179.

41. Casanova-Sepúlveda, G., Sexton, J.A., Turk, B.E., and Boggon, T.J. (2023). Autoregulation of the LIM kinases by their PDZ domain. Nat. Commun. *14*, 8441. https://doi.org/10.1038/s41467-023-44148-4.

42. McDermaid, A., Monier, B., Zhao, J., Liu, B., and Ma, Q. (2019). Interpretation of differential gene expression results of RNA-seq data: review and integration. Brief. Bioinform. *20*, 2044–2054. https://doi.org/10.1093/bib/bby067.

43. Sasca, D., Szybinski, J., Schüler, A., Shah, V., Heidelberger, J., Haehnel, P.S., Dolnik, A., Kriege, O., Fehr, E.-M., Gebhardt, W.H., et al. (2019). NCAM1 (CD56) promotes leukemogenesis and confers drug resistance in AML. Blood *133*, 2305–2319. https://doi.org/10.1182/blood-2018-12-889725.

44. Walmod, P.S., Kolkova, K., Berezin, V., and Bock, E. (2004). Zippers make signals: NCAM-mediated molecular interactions and signal transduction. Neurochem. Res. *29*, 2015–2035. https://doi.org/10.1007/s11064-004-6875-z.

45. Hallgren, J., Tsirigos, K.D., Pedersen, M.D., Almagro Armenteros, J.J., Marcatili, P., Nielsen, H., Krogh, A., and Winther, O. (2022). DeepTMHMM predicts alpha and beta transmembrane proteins using deep neural networks. Preprint at bioRxiv. https://doi.org/10.1101/2022.04.08.487609.

46. Abramson, J., Adler, J., Dunger, J., Evans, R., Green, T., Pritzel, A., Ronneberger, O., Willmore, L., Ballard, A.J., Bambrick, J., et al. (2024). Accurate structure prediction of biomolecular interactions with AlphaFold 3. Nature *630*, 493–500. https://doi.org/10.1038/s41586-024-07487-w.

47. Hasel, P., Rose, I.V.L., Sadick, J.S., Kim, R.D., and Liddelow, S.A. (2021). Neuroinflammatory astrocyte subtypes in the mouse brain. Nat. Neurosci. *24*, 1475–1487. https://doi.org/10.1038/s41593-021-00905-6.

48. Frazel, P.W., Labib, D., Fisher, T., Brosh, R., Pirjanian, N., Marchildon, A., Boeke, J.D., Fossati, V., and Liddelow, S.A. (2023). Longitudinal scRNA-seq analysis in mouse and human informs optimization of rapid mouse astrocyte differentiation protocols. Nat. Neurosci. *26*, 1726–1738. https://doi.org/10.1038/s41593-023-01424-2.

49. Lu, Y., Yue, D., Xie, J., Cheng, L., and Wang, X. (2022). Ontology Specific Alternative Splicing Changes in Alzheimer's Disease. Front. Genet. *13*, 926049. https://doi.org/10.3389/fgene.2022.926049.

50. Lu, Y., Tan, L., Xie, J., Cheng, L., and Wang, X. (2022). Distinct microglia alternative splicing in Alzheimer's disease. Aging (Albany NY) *14*, 6554–6566. https://doi.org/10.18632/aging.204223.

51. Jankowsky, J.L., and Zheng, H. (2017). Practical considerations for choosing a mouse model of Alzheimer's disease. Mol. Neurodegener. *12*, 89. https://doi.org/10.1186/s13024-017-0231-7.

52. Zhong, M.Z., Peng, T., Duarte, M.L., Wang, M., and Cai, D. (2024). Updates on mouse models of Alzheimer's disease. Mol. Neurodegener. *19*, 23. https://doi.org/10.1186/s13024-024-00712-0.

53. Nikom, D., and Zheng, S. (2023). Alternative splicing in neurodegenerative disease and the promise of RNA therapies. Nat. Rev. Neurosci. *24*, 457–473. https://doi.org/10.1038/s41583-023-00717-6.

54. Vukojevic, V., Mastrandreas, P., Arnold, A., Peter, F., Kolassa, I.-T., Wilker, S., Elbert, T., de Quervain, D.J.F., Papassotiropoulos, A., and Stetak, A. (2020). Evolutionary conserved role of neural cell adhesion molecule-1 in memory. Transl. Psychiatry *10*, 217. https://doi.org/10.1038/s41398-020-00899-y.

55. Farhadieh, M.-E., and Ghaedi, K. (2023). Analyzing alternative splicing in Alzheimer's disease postmortem brain: a cell-level perspective. Front. Mol. Neurosci. *16*, 1237874. https://doi.org/10.3389/fnmol.2023.1237874.

56. Escartin, C., Galea, E., Lakatos, A., O'Callaghan, J.P., Petzold, G.C., Serrano-Pozo, A., Steinhäuser, C., Volterra, A., Carmignoto, G., Agarwal, A., et al. (2021). Reactive astrocyte nomenclature, definitions, and future directions. Nat. Neurosci. *24*, 312–325. https://doi.org/10.1038/s41593-020-00783-4.

57. Bernhem, K., Blom, H., and Brismar, H. (2018). Quantification of endogenous and exogenous protein expressions of Na,K-ATPase with super-resolution PALM/STORM imaging. PLoS One *13*, e0195825. https://doi.org/10.1371/journal.pone.0195825.

58. Prelich, G. (2012). Gene overexpression: uses, mechanisms, and interpretation. Genetics *190*, 841–854. https://doi.org/10.1534/genetics.111.136911.

59. Dobin, A., Davis, C.A., Schlesinger, F., Drenkow, J., Zaleski, C., Jha, S., Batut, P., Chaisson, M., and Gingeras, T.R. (2013). STAR: ultrafast universal RNA-seq aligner. Bioinformatics *29*, 15–21. https://doi.org/10.1093/bioinformatics/bts635.

60. Li, B., and Dewey, C.N. (2011). RSEM: accurate transcript quantification from RNA-Seq data with or without a reference genome. BMC Bioinf. *12*, 323. https://doi.org/10.1186/1471-2105-12-323.

61. Liao, Y., Smyth, G.K., and Shi, W. (2014). featureCounts: an efficient general purpose program for assigning sequence reads to genomic features. Bioinformatics *30*, 923–930. https://doi.org/10.1093/bioinformatics/btt656.

62. Love, M.I., Huber, W., and Anders, S. (2014). Moderated estimation of fold change and dispersion for RNA-seq data with DESeq2. Genome Biol. *15*, 550. https://doi.org/10.1186/s13059-014-0550-8.

63. Wang, Y., Xie, Z., Kutschera, E., Adams, J.I., Kadash-Edmondson, K.E., and Xing, Y. (2024). rMATS-turbo: an efficient and flexible computational tool for alternative splicing analysis of large-scale RNA-seq data. Nat. Protoc. *19*, 1083–1104. https://doi.org/10.1038/s41596-023-00944-2.

64. Ascensão-Ferreira, M., Martins-Silva, R., Saraiva-Agostinho, N., and Barbosa-Morais, N.L. (2024). betAS: intuitive analysis and visualization of differential alternative splicing using beta distributions. RNA *30*, 337–353. https://doi.org/10.1261/rna.079764.123.

65. Liebermeister, W., Noor, E., Flamholz, A., Davidi, D., Bernhardt, J., and Milo, R. (2014). Visual account of protein investment in cellular functions. Proc. Natl. Acad. Sci. USA *111*, 8488–8493. https://doi.org/10.1073/pnas.1314810111.

66. Zhou, Y., Zhou, B., Pache, L., Chang, M., Khodabakhshi, A.H., Tanaseichuk, O., Benner, C., and Chanda, S.K. (2019). Metascape provides a biologist-oriented resource for the analysis of systems-level datasets. Nat. Commun. *10*, 1523. https://doi.org/10.1038/s41467-019-09234-6.

67. Mistry, J., Chuguransky, S., Williams, L., Qureshi, M., Salazar, G.A., Sonnhammer, E.L.L., Tosatto, S.C.E., Paladin, L., Raj, S., Richardson, L.J., et al. (2021). Pfam: The protein families database in 2021. Nucleic Acids Res. *49*, D412–D419. https://doi.org/10.1093/nar/gkaa913.

68. Vitting-Seerup, K., and Sandelin, A. (2019). IsoformSwitchAnalyzeR: analysis of changes in genome-wide patterns of alternative splicing and its functional consequences. Bioinformatics *35*, 4469–4471. https://doi.org/10.1093/bioinformatics/btz247.

69. Zheng, G.X.Y., Terry, J.M., Belgrader, P., Ryvkin, P., Bent, Z.W., Wilson, R., Ziraldo, S.B., Wheeler, T.D., McDermott, G.P., Zhu, J., et al. (2017). Massively parallel digital transcriptional profiling of single cells. Nat. Commun. *8*, 14049. https://doi.org/10.1038/ncomms14049.

70. Hao, Y., Stuart, T., Kowalski, M.H., Choudhary, S., Hoffman, P., Hartman, A., Srivastava, A., Molla, G., Madad, S., Fernandez-Granda, C., and Satija, R. (2024). Dictionary learning for integrative, multimodal and scalable single-cell analysis. Nat. Biotechnol. *42*, 293–304. https://doi.org/10.1038/s41587-023-01767-y.

71. Hu, C., Li, T., Xu, Y., Zhang, X., Li, F., Bai, J., Chen, J., Jiang, W., Yang, K., Ou, Q., et al. (2023). CellMarker 2.0: an updated database of manually curated cell markers in human/mouse and web tools based on scRNA-seq data. Nucleic Acids Res. *51*, D870–D876. https://doi.org/10.1093/nar/gkac947.

72. Wen, W.X., Mead, A.J., and Thongjuea, S. (2023). MARVEL: an integrated alternative splicing analysis platform for single-cell RNA sequencing data. Nucleic Acids Res. *51*, e29. https://doi.org/10.1093/nar/gkac1260.

73. Schneider, C.A., Rasband, W.S., and Eliceiri, K.W. (2012). NIH Image to ImageJ: 25 years of image analysis. Nat. Methods *9*, 671–675. https://doi.org/10.1038/nmeth.2089.

STAR★METHODS

KEY RESOURCES TABLE

REAGENT or RESOURCE	SOURCE	IDENTIFIER
Antibodies		
Rabbit polyclonal anti-NCAM1/CD56	Proteintech	Cat#14255-1-AP; RRID: AB_2149421
Deposited data		
The raw bulk RNA-seq data	https://www.ncbi.nlm.nih.gov/geo/query/acc.cgi?acc=GSE173955	GSE173955
The raw single nucleus RNA -seq data	https://www.ncbi.nlm.nih.gov/geo/query/acc.cgi?acc=GSE221959	GSE221959
Experimental models: Organisms/strains		
Mouse: C57BL/6J male mice	Jiangsu Huachuang Xinnuo Pharmaceutical Technology Co., Ltd.	N/A
Mouse: APP/PS1 transgenic male mice (C57BL/6J-Tg (APPswe, PSEN1dE9))	Hangzhou Ziyuan Laboratory Animal Technology Co., Ltd.	N/A
Oligonucleotides		
L-Ncam1 Mouse RT PCR Primers; Forward:5′-CCGAAAAGGGCCCTGTAGAA-3′, Reverse:5′- GGGGACCGTCTTGACTTCAG-3′	This paper	N/A
S-Ncam1 Mouse RT PCR Primers; Forward:5′-GGCAGCTCACTTTGTGTTCA-3′, Reverse:5′- AGTCACCGCAGAGAAAAGCAA-3′	This paper	N/A
Gapdh Mouse RT PCR Primers; Forward:5′-TGGCCTTCCGTGTTCCTAC-3′, Reverse:5′- GAGTTGCTGTTGAAGTCGCA-3′	This paper	N/A
Software and algorithms		
RStudio (version 4.3.2)	RStudio Team	https://www.rstudio.com/
RSEM (version 1.3.1)	Li et al.[1]	https://github.com/deweylab/RSEM
Proteomaps	Liebermeister et al.[2]	https://github.com/eladnoor/proteomaps
ggplot2 (version 3.4.2)	Wickham et al.	https://ggplot2.tidyverse.org
STAR (version 2.4.11a)	Dobin et al.[3]	https://github.com/alexdobin/STAR
feature Counts (version 2.0.6)	Liao et al.[4]	https://subread.sourceforge.net/featureCounts.html
IsoformSwitchAnalyzeR	Vitting et al.[5]	https://github.com/kvittingseerup/IsoformSwitchAnalyzeR
DESeq2 (version 1.50.2)	Love et al.[6]	https://github.com/thelovelab/DESeq2
Metascape (version 3.5)	Zhou et al.[7]	https://metascape.org/gp
rMATS (version 1.32.0)	Wang et al.[8]	https://github.com/Xinglab/rmats-turbo
rmats2sashimiplot (v3.0.0)	Xing et al.	https://github.com/Xinglab/rmats2sashimiplot
betAS (version 1.2.1)	Ferreira et al.[9]	https://github.com/DiseaseTranscriptomicsLab/betAS
GraphPad Prism (version 8.0.2)	GraphPad Software Inc.	https://www.graphpad.com/
Image J	Schneider et al.[10]	https://imagej.nih.gov/ij/
Pfam_scan (version 1.0)	Mistry et al.[11]	https://github.com/aziele/pfam_scan
Cell Ranger (version 7.1.0)	Zheng et al.[12]	https://github.com/10XGenomics/cellranger
Seurat (version 1.2.1)	Hao et al.[13]	https://github.com/satijalab/seurat
CellMarker2.0	Hu et al.[14]	http://117.50.127.228/CellMarker/
MARVEL (version 2.0.5)	Wen et al.[15]	https://github.com/wenweixiong/MARVEL/

CellPress
OPEN ACCESS

EXPERIMENTAL MODEL AND STUDY PARTICIPANT DETAILS

AD mouse model

A total of 40 male mice, including 20 wild-type C57BL/6J mice and 20 APP/PS1 transgenic mice, were used in this study. The C57BL/6J mice, aged 6 months and weighing 30-35g, were purchased from Jiangsu HuachuangXinnuo Pharmaceutical Technology Co., Ltd. The APP/PS1 mice, also aged 6 months and weighing 30-35g, were purchased from Hangzhou Ziyuan Laboratory Animal Technology Co., Ltd. All mice were housed in a controlled environment with a 12-hour light/dark cycle and allowed free access to standard rodent chow and water. The animals were acclimated to the laboratory conditions for at least 1 week before the start of the experiment. All animal procedures were conducted in accordance with institutional and national guidelines and were approved by the Institutional Animal Care and Use Committee of the Pharmaceutical Laboratory Animal Center at China Pharmaceutical University (Approval No. 2025-03-003).

METHOD DETAILS

Transcriptome assembly and quantification from RNA-seq data

The bulk RNA-seq data from 18 human hippocampal tissue samples (8 individuals diagnosed with AD and 10 non-AD controls) were obtained under accession number GSE173955, and all individuals included in the dataset were older than 60 years. These sequencing data were aligned to the human reference genome (hg38) with the STAR aligner (version 2.4.11a),[59] employing a two-step mapping approach that integrates splice junction information from each sample. Following the initial phase of mapping, an updated indexing strategy for identified splice junctions was generated, excluding splice junctions originating from mitochondrial DNA, non-canonical junctions, and those with inadequate read support (read counts < 3), generating the results with heightened precision and accuracy. After this two-stage approach alignment, the data were analyzed with featureCounts (version 2.0.6) and RSEM (version 1.3.1) for transcript assembly,[60,61] utilizing ENSEMBL GRCh38 and GRCm39 annotations as a guide for the transcript model reference. To assess differential gene expression, DESeq2 (version 1.32.0) was employed,[62] applying stringent criteria that mandated a P-value < 0.05 and an absolute log2 fold change ($|\log2FC| > 1$ for the identification of gene-level differentially expressed genes (DEGs) and differentially expressed transcripts. Conversely, genes deemed not differentially expressed at the gene level (nDEGs) were identified based on either an absolute log2 fold change ($|\log2FC| < 1$ or a P-value > 0.05.

Analysis of AS events

In brief, consistent with previous studies, AS events were classified into five distinct categories: exon skipping (ES), mutually exclusive exons (MXE), alternative 3′ splice sites (A3SS), alternative 5′ splice sites (A5SS), and intron retention (IR). The inclusion ratios of alternative exons or introns were quantified using rMATS (version 1.32.0) and betAS (version 1.2.1).[63,64] AS events were considered significant between AD patients and non-AD controls if $|\Delta PSI| \geq 0.10$, a commonly used and conservative effect-size cutoff in differential splicing analyses.[63] P-values were calculated by rMATS and adjusted for multiple testing using the Benjamini–Hochberg procedure, with FDR < 0.01 indicating significance. For representative genes and splicing events, sashimi plots were generated using the rmats2sashimiplot utility to visualize exon–exon junction usage and splicing patterns across conditions.

Functional enrichment analysis

To explore the biological functions of gene-level non-differentially expressed genes (nDEGs), we analyzed their Transcripts Per Million (TPM) values, which were used as inputs for Proteomaps analysis.[65] Additionally, we employed Metascape tools to enrich the functional profiles of genes exhibiting AS.[66] For skipped exon genes with no changes in expression levels, we conducted domain analysis using Pfam.[67]

Isoform switching analysis

Isoform switching analysis was performed using IsoformSwitchAnalyzeR (version 2.2.0).[68] To determine the change of isoform levels, we assessed the difference in isoform fraction (dIF) between AD and non-AD cohorts. We established a criterion for statistical significance, considering a switch to be notable when the difference in isoform fraction (dIF) exceeded 0.1 and was accompanied by a P-value below 0.05, indicating robust evidence for isoform switching.

Single nucleus RNA sequencing analysis

The single-nucleus RNA-seq data from 12 mouse hippocampal samples (6 WT and 6 AD-BXD mice) were obtained under accession number GSE221959, and all mice included in the dataset were 14 months old. Firstly, the sequencing reads were mapped according to the GRCm39 mouse reference genome using the 10x Genomics Cell Ranger (version 7.1.0),[69] and then processed using STARsolo,[59] generating gene expression count matrices. To ensure data quality, we implemented rigorous quality control measures within Seurat (version 1.2.1),[70] excluding cells with excessive mitochondrial gene content ($> 15\%$) or genes expressed in fewer than 10 cells. After data washing, the expression data was normalized to account for library size differences, scaling Unique Molecular Identifier (UMI) counts to a uniform total of 10,000 per cell. Substantially, we integrated the data and calculated t-distributed Stochastic Neighbor Embedding (t-SNE) coordinates for dimensional reduction and visualization purposes. Cell types were manually

annotated by referencing the CellMarker2.0 database.[71] Finally, to unravel AS events at single-nucleus resolution, we applied MARVEL (version 2.0.5) to capture the intricate landscape of alternative splicing. We excluded non–protein-coding genes from downstream analyses. For differential splice-site usage, only genes expressed in ≥10% of cells and splice junctions detected in ≥10% of cells were retained for downstream AS analyses. Differential splicing was assessed using MARVEL's bootstrap-based testing framework, which estimates the significance of splicing differences by resampling PSI distributions across cells within each group. Given the increased technical noise and sparsity inherent to single-nucleus data, we applied relatively permissive thresholds, defining significant AS events as those with P-value < 0.05 and $|\Delta PSI| > 0.05$.[72] All single-cell analyses were performed using the integrated Seurat object. Cell type–specific Ncam1 expression levels were calculated as the total Ncam1 expression across all cells of a given cell type divided by the total number of cells in that cell type. For S-NCAM1, a specific splice junction was used as a marker, and S-NCAM1 expression was defined based on the presence of this splice junction, calculated as the total number of cells containing the specific intron junction divided by the total number of Ncam1-expressing cells.

Western blot assay

The mice were humanely euthanized under deep anesthesia. To ensure complete perfusion, cold PBS was pumped through the left ventricle at a controlled flow rate of 10 mL/min for a duration of 60 seconds. Following cardiac perfusion, brains were meticulously extracted, and total cellular proteins were extracted from the hippocampal tissues. This was done by lysing the tissues with RIPA buffer (purchased from Beyotime) supplemented with phenylmethylsulfonyl fluoride (PMSF). Subsequently, the lysates were centrifuged at 12,000 rpm/min at 4°C for 30 minutes to collect the supernatant. The quantification of protein content was performed using a BCA kit (also obtained from Beyotime). The isolated proteins were subjected to electrophoresis on SDS-PAGE (sodium dodecyl sulfate-polyacrylamide gel electrophoresis) and then transferred onto polyvinylidene difluoride (PVDF) membranes (purchased from Millipore). After transfer, the membranes were blocked with 5% skim milk prepared in Tris-buffered saline containing 0.1% Tween 20 (TBST) for 1 hour at room temperature. The membranes were then incubated overnight at 4°C with primary antibodies, appropriately diluted in blocking solution, including the NCAM1 antibody purchased from Proteintech (Wuhan, China). After thorough washing with TBST for five cycles, the membranes were incubated with secondary antibodies (HRP-conjugated anti-rabbit IgG) for 1 hour at room temperature. Protein expression was detected using an enhanced chemiluminescence kit (Tanon) and visualized using a Gel Imaging System (Bio-Rad, ChemiDoc MP, USA). The resulting densitometry values were normalized to the intensity levels of tubulin, and quantification was performed using ImageJ.[73]

RNA isolation and RT–qPCR analysis

Hippocampal tissues were dissected from APP/PS1 mice, and total RNA was extracted using RNA isolater Total RNA Extraction Reagent (Vazyme) according to the manufacturer's instructions. RNA was reverse-transcribed into cDNA using HiScript II Reverse Transcriptase (Vazyme) on a Gene Explorer thermal cycler (BIOER). Quantitative real-time PCR (qPCR) was performed on a CFX Opus 384 system (Bio-Rad) using SYBR Green PCR Master Mix (Vazyme). The thermal cycling conditions consisted of an initial denaturation at 95°C for 10 min, followed by 35 cycles of 95°C for 15 s, 60°C for 30 s, and 72°C for 30 s. Isoform-specific primers were designed to selectively amplify total *Ncam1*, L-*Ncam1*, and S-*Ncam1* transcript isoforms. Quantitative real-time PCR was performed to quantify total *Ncam1* expression as well as individual isoforms. Isoform switching was assessed by calculating the ratio of L-*Ncam1* to S-*Ncam1* expression levels. Relative expression levels were calculated using the $2^{-\Delta\Delta Ct}$ method and normalized to an endogenous control.

QUANTIFICATION AND STATISTICAL ANALYSIS

Transcriptomic differential expression analysis was performed in R studio (version 4.3.2), where P-values were calculated using DESeq2 (version 1.50.2). Statistical analyses and data visualization for biological experiments, including RT-qPCR and Western blot analyses, were performed using GraphPad Prism 9. Sample sizes correspond to the number of biological replicates and are reported in the figure legends and Results. Data are presented as mean ± SEM. Differences between two groups were assessed using an unpaired two-tailed Student's t-test. Full statistical details, including exact sample sizes and significance values, are provided in the figure legends and main text.